Tumor Biology and Immunology: *Resource Report*

Cancer Research

Comprehensive Phenotypic Characterization of Human Invasive Lobular Carcinoma Cell Lines in 2D and 3D Cultures

Nilgun Tasdemir[1,2], Emily A. Bossart[1,2], Zheqi Li[1,2], Li Zhu[3], Matthew J. Sikora[4], Kevin M. Levine[1,5], Britta M. Jacobsen[4], George C. Tseng[3,6], Nancy E. Davidson[7,8], and Steffi Oesterreich[1,2]

Abstract

Invasive lobular carcinoma (ILC) is the second most common subtype of breast cancer following invasive ductal carcinoma (IDC) and characterized by the loss of E-cadherin–mediated adherens junctions. Despite displaying unique histologic and clinical features, ILC still remains a chronically understudied disease, with limited knowledge gleaned from available laboratory research models. Here we report a comprehensive 2D and 3D phenotypic characterization of four estrogen receptor–positive human ILC cell lines: MDA-MB-134, SUM44, MDA-MB-330, and BCK4. Compared with the IDC cell lines MCF7, T47D, and MDA-MB-231, ultra-low attachment culture conditions revealed remarkable anchorage independence unique to ILC cells, a feature not evident in soft-agar gels. Three-dimensional Collagen I and Matrigel culture indicated a generally loose morphology for ILC cell lines, which exhibited differing preferences for adhesion to extracellular matrix proteins in 2D. Furthermore, ILC cells were limited in their ability to migrate and invade in wound-scratch and transwell assays, with the exception of haptotaxis to Collagen I. Transcriptional comparison of these cell lines confirmed the decreased cell proliferation and E-cadherin–mediated intercellular junctions in ILC while uncovering the induction of novel pathways related to cyclic nucleotide phosphodiesterase activity, ion channels, drug metabolism, and alternative cell adhesion molecules such as N-cadherin, some of which were differentially regulated in ILC versus IDC tumors. Altogether, these studies provide an invaluable resource for the breast cancer research community and facilitate further functional discoveries toward understanding ILC, identifying novel drug targets, and ultimately improving the outcome of patients with ILC.

Significance: These findings provide the breast cancer research community with a comprehensive assessment of human invasive lobular carcinoma (ILC) cell line signaling and behavior in various culture conditions, aiding future endeavors to develop therapies and to ultimately improve survival in patients with ILC. *Cancer Res; 78(21); 6209–22. ©2018 AACR.*

Introduction

Invasive lobular carcinoma (ILC) is the second most common type of breast cancer following invasive ductal carcinoma (IDC), accounting for 10%–15% of all cases (1). At an annual number of approximately 25–38,000, which is higher than ovarian cancer or melanoma, ILC is the sixth most common cancer among women in United States (2). Histologically, IDC tumors form palpable masses or lumps, while ILCs grow as small, dyscohesive cells in a single-file pattern (1, 3). This unique growth pattern makes mammographic detection and surgical removal of ILC difficult, complicating breast conservation (3). In addition, compared with IDCs, ILCs present more frequently as multicentric and bilateral and with metastases to ovaries, peritoneum, and gastrointestinal tract (1, 4). Paradoxically, while patients with ILC display favorable prognostic and predictive factors [estrogen receptor (ER)-positive, progesterone receptor-(PR) positive, HER2-negative, low Ki67 index] and are mostly treated with endocrine therapy, they exhibit more long-term recurrences compared with patients with IDC, indicative of endocrine resistance (4, 5).

Despite its distinctive histologic and clinical features, ILC has remained a gravely understudied subtype of breast cancer. The most characteristic feature of ILC is the lack of E-cadherin–mediated adherens junctions, thought to be largely responsible for its single-file growth pattern (6). This hallmark E-cadherin loss, found in 95% of all ILC tumors versus in only 7% of IDCs, occurs through truncating mutations and loss-of-heterozygosity (6–12). Our knowledge of ILC as a unique subtype of breast cancer is only recently emerging with

[1]Women's Cancer Research Center, University of Pittsburgh Medical Center (UPMC) Hillman Cancer Center (HCC), Magee-Womens Research Institute, Pittsburgh, Pennsylvania. [2]Department of Pharmacology & Chemical Biology, University of Pittsburgh, Pittsburgh, Pennsylvania. [3]Department of Biostatistics, University of Pittsburgh, Pittsburgh, Pennsylvania. [4]Dept. of Pathology, University of Colorado Anschutz Medical Campus, Aurora, Colorado. [5]Department of Pathology, University of Pittsburgh, Pittsburgh, Pennsylvania. [6]Department of Computational & Systems Biology, Pittsburgh, Pennsylvania. [7]Fred Hutchinson Cancer Center, Seattle, Washington. [8]University of Washington, Seattle, Washington.

Note: Supplementary data for this article are available at Cancer Research Online (http://cancerres.aacrjournals.org/).

Corresponding Author: Steffi Oesterreich, Women's Cancer Research Center, UPMC Hillman Cancer Center, 204 Craft Avenue, Pittsburgh, PA 15213. Phone: 412-641-8555; Fax: 412-641-7724; E-mail: oesterreichs@upmc.edu

doi: 10.1158/0008-5472.CAN-18-1416

comprehensive reports from big consortia such as The Cancer Genome Atlas (TCGA; ref. 7) and Rational Therapy for Breast Cancer (RATHER; ref. 13). Multi-omics profiling of human tumors has begun to reveal candidate disease drivers such as *HER2*, *HER3*, *FOXA1*, and *PIK3CA* mutations, *PTEN* loss, and *ESR1* amplifications, events more frequently observed in ILC compared with IDC (7, 13, 14). However, the functional validation of these potential drivers is hindered by the availability of few ER-positive human ILC cell lines for use in the laboratory and limited knowledge on their biological phenotypes. Thus, there is urgent need to develop additional cell line models, as well as thoroughly characterizing the cellular behaviors of the existing ones.

Our laboratory has recently reported the first profiling of ER function and endocrine response in ER-positive human ILC cell lines (15). Here we go one step beyond and characterize their growth and morphologies in 3D environments such as in ultra-low attachment (ULA) culture (16), soft agar (17), and within/on top of extracellular matrix (ECM) proteins (18, 19), as well as their adhesion properties in 2D (20). Using IDC cell lines for comparison, we probe their migration potential in response to both soluble attractants in chemotaxis assays (21) and to substrate-bound ECM proteins in haptotaxis assays (22). In addition, we report on their abilities to invade Collagen I and Matrigel, as well as assessing their use of amoeboid invasion in non-cross-linked Collagen I gels (23, 24). Comparison of transcriptional profiling data of ER-positive human ILC and IDC cell lines identified a number of clinically relevant genes and pathways that provide important insights into the subtype-specific gene expression programs likely responsible for their divergent biological phenotypes. Combined, our studies serve as an invaluable resource for modeling ILC in the laboratory and pave the way for a promising direction of research for ILC biology toward new discoveries.

Materials and Methods

Cell culture

MDA-MB-134-VI (MDA-MB-134), MDA-MB-330, MCF-7, T47D and MDA-MB-231 were obtained from the ATCC. SUM44PE (SUM44) was purchased from Asterand and BCK4 cells were developed as reported previously (25). Cell lines were maintained in the following media (Life Technologies) with 10% FBS: MDA-MB-134 and MDA-MB-330 in 1:1 DMEM:L-15, MCF7 and MDA-MB-231 in DMEM, T47D in RPMI, and BCK4 in MEM with nonessential amino acids (Life Technologies) and insulin (Sigma-Aldrich). SUM44 was maintained as described previously (15) in DMEM-F12 with 2% charcoal-stripped serum and supplements. Cell lines were routinely tested to be *Mycoplasma* free, authenticated by the University of Arizona Genetics Core by short tandem repeat DNA profiling and kept in continuous culture for <6 months. Estrogen and antiestrogen treatments were done on hormone-deprived cells as described previously (15). PIK3CA plasmids in pBABE (Addgene) and PTEN shRNAs in pMLPE (a kind gift from Scott W. Lowe, Memorial Sloan Kettering Cancer Center, New York, NY) were packaged as described previously (26) and cells were selected with 1 μg/mL puromycin (Life Technologies). shRNA sequences are provided in Supplementary Table S1.

Immunoassays and trichrome staining

Western blots were performed as described previously (27) using 5% milk powder for blocking and developed using ECL (Sigma-Aldrich). For immunofluorescence, cells grown on coverslips were fixed with 4% paraformaldehyde, permeabilized, and blocked with 5% normal goat serum. Coverslips were incubated with antibodies, washed, and mounted using DAPI-containing media (Thermo Fisher Scientific). Slides were imaged using a Nikon A1 advanced confocal system. Details of the antibodies used are included in Supplementary Table S1. Masson's Trichrome (Sigma-Aldrich) staining was performed on a tissue microarray using manufacturer's protocol without the acetic acid step after the aniline blue.

Proliferation, anchorage independence, and stemness assays

Estrogen and antiestrogen treatment-induced growth assays were done and quantified using FluoReporter dsDNA quantitation kit (Life Technologies) as described previously (15). For 2D and ULA growth assays, ILC (15,000/96-well; 300,000/6-well) and IDC (5,000/96-well; 100,000/6-well) cells were seeded in regular (Thermo Fisher Scientific) or ULA (Corning Life Sciences) 96-well plates and assayed using CellTiter-Glo (Promega) on a Promega GloMax plate reader. Soft agar assays with ILC (50,000/plate) and IDC (10,000/plate) cells were performed in 35-mm plates (Thermo Fisher Scientific) as described previously (17, 28). For mammosphere assays, ILC (60,000/well) and IDC (20,000/well) cells were seeded in 6-well ULA plates (Corning Life Sciences) as described previously (29) in 1:1 DMEM/Ham F-12 media with 20 ng/mL bFGF (BD Biosciences), 20 ng/mL EGF (BD Biosciences), B27 (Gibco), 2.5 mL penicillin/streptomycin, and 4 μg/mL heparin (Sigma-Aldrich). All images were taken on an Olympus IX83 inverted microscope. For stem cell expression experiments, cells were stained with the indicated antibodies and analyzed on an LSRII flow cytometer (BD Biosciences). Gating was performed using the BD FACS Diva Software and isotype antibody stainings. Details of the antibodies used are included in Supplementary Table S1.

RNA extraction, quantitative PCR, and NanoString gene expression analyses

RNA extraction, qRT-PCRs, and NanoString analyses were done as described previously (15).

3D ECM assays

ILC (15,000/well) and IDC (5,000) cells were embedded in rat tail Collagen I (Corning Life Sciences) at 4 mg/mL in 24-well plates following manufacturer's recommendations. For Matrigel (BD Biosciences) assays, ILC (5,000/well) and IDC (4,000/well) cells were seeded into single wells of 8-well LabTek Chamber Slides (Thermo Fisher Scientific) as described previously (18). Colonies were imaged on an Olympus IX83 inverted microscope.

ECM adhesion assays

ILC ($1–2 \times 10^5$ cells/well) and IDC ($5 \times 10^4–1 \times 10^5$ cells/well) cells were seeded into 96-well plates with the indicated coatings (Corning Life Sciences) following detachment with PBS containing 2 mmol/L EDTA. After incubation, plates were imaged on an Olympus IX83 inverted microscope, washed twice with PBS, and quantified using FluoReporter dsDNA kit (Life Technologies) following the manufacturer's protocol.

Migration and invasion assays

Wound-scratch assays were performed as described previously (30, 31) using the IncuCyte Zoom Live Cell Imaging

System (Essen Bioscience). Phorbol myristate acetate (PMA; Sigma-Aldrich) was used at 100 nmol/L. For transwell experiments, cells were serum starved overnight, plated into 8-μm inserts (Thermo Fisher Scientific and Cell Biolabs), and quantified using Crystal violet following manufacturer's protocol. Images of inserts were taken on an Olympus SZX16 dissecting microscope.

Differential gene expression, pathway, and survival analyses

RNA-Sequencing data of the cell lines was obtained from Marcotte and colleagues (32). The R package DESeq2 was used for differential expression analysis and pathway enrichment analysis was implemented using KEGG, BIOCARTA, REACTOME, and KEGG databases as described previously (27). Survival analysis was performed using the METABRIC dataset (33) as described previously (27).

Statistical analysis

Statistical analysis was performed using GraphPad Prism. Data are presented as mean ± SD. Statistical tests used for each figure are indicated in the respective figure legends.

Supplementary methods

Detailed methods are described in Supplementary text.

Results

Hormone receptor and adherens junction status

In this study, we focused on four ER-positive human ILC cell lines (MDA-MB-134, SUM44, MDA-MB-330, and BCK4) and utilized the IDC cell lines MCF7, T47D, and MDA-MB-231 for comparative studies. As seen in Fig. 1A, Western blotting confirmed ER expression in all cell lines, except for the ER-negative MDA-MB-231 cells (34). Of note, although there are conflicting reports on the ER status of MDA-MB-330 cells (34, 35), they displayed abundant ER levels in our hands. Only BCK4 and T47D had detectable PR expression at these exposure conditions. We have previously reported partial tamoxifen agonism in MDA-MB-134 and ligand-independent ER pathway activation in SUM44 cells (15). Extension of this analysis to the remaining ER-positive ILC cell lines revealed that estradiol does not induce growth in MDA-MB-330 cells despite regulating ER target genes (Fig. 1B, Supplementary Fig. S1A), while tamoxifen also acts as a partial agonist in BCK4 cells (Fig. 1C; Supplementary Fig. S1B–S1E).

As expected, E-cadherin was absent from MDA-MB-134, SUM44, which harbor *CDH1* truncating mutations (35), from BCK4 cells, as well as from MDA-MB-231 cells, in which the *CDH1* promoter is hypermethylated (Fig. 1A; ref. 36). Consistent with the downregulation and/or mislocalization of other junction components in the absence of E-cadherin (37, 38), β-catenin expression was not detected in MDA-MB-134, SUM44, and BCK4 cells, a result different from that in MDA-MB-231 cells, which retained β-catenin expression without E-cadherin. Interestingly, MDA-MB-330 cells, which harbor a biallelic, truncating *CTNNA1* mutation (35), still expressed E-cadherin and β-catenin in the absence of α-catenin. In contrast, p120-catenin (p120) was detected in all cell lines with the weakest expression in BCK4 cells, which also exhibited lower α-catenin levels. Coimmunofluorescence staining confirmed the absence of functional E-cadherin in ILC cell lines, which was mislocalized to the cytoplasm in MDA-MB-330 cells (Fig. 1D, top; Supplementary Fig. S2). Similarly, p120 was also largely cytoplasmic in ILC cell lines and in MDA-MB-231 cells, unlike its normal membranous colocalization with E-cadherin in IDC cells (Fig. 1D; bottom; Supplementary Fig. S2). Collectively, these data confirm the absence of functional adherens junctions in ILC cells.

Anchorage-independent ability

Next we assessed the anchorage-independent ability of ILC cell lines by growing them in ULA conditions, which forces them into a suspension culture (16). ILC cell lines exhibited a dyscohesive, scattered morphology in 2D plates consistent with their lack of adherens junctions, while growing as large floating clusters in ULA plates (Fig. 2A, top). In contrast, MCF7 and T47D cells were more cohesive in 2D and formed tight spheres in ULA (Fig. 2A, bottom). Despite having overall slower proliferation rates compared with the IDC cells, the ILC cell lines had a remarkable ability to grow equally well in 2D and ULA plates, with BCK4 showing the least robust ULA phenotype (Fig. 2B). Importantly, this anchorage independence was unique to the ILC cells, as the IDC cell lines had much poorer growth in ULA versus 2D culture. Interestingly, while MDA-MB-231 cells with no adherens junctions displayed a loose ULA morphology more similar to ILC than IDC cells, they had the poorest ULA growth of all the IDC cell lines.

Given the superior anchorage-independent growth of ILC cell lines compared with IDC, we also assessed their ability to form mammospheres, which are similarly grown in ULA plates but with a selective media that enriches for stem-like cells (29). Assessment of stemness in the ILC cell lines was also of interest to us given the higher expression of stem cell markers such as ALDH1A1 in ILC versus IDC tumors (39, 40). Despite their robust growth in ULA conditions, ILC cell lines formed poorly defined, loose mammospheres that were difficult to quantify, unlike the tighter MCF7 and T47D spheres (Supplementary Fig. S3A). Flow cytometric analysis of stem cell markers similarly did not identify a putative $CD24^{low}/CD44^{high}$ or $CD49f^{high}/EPCAM^{low}$ stem cell population in the ILC cell lines (Supplementary Fig. S3B and S3C). Although such a population was present in MDA-MB-231 cells, this cell line did not form mammospheres as robustly as MCF7 and T47D cells. Consistent with previous literature, these results indicate poor mammosphere formation in cells with disrupted adherens junctions and a discordance between stem cell expression and mammosphere formation ability (41).

Another form of anchorage independence is the ability to grow in suspension in soft-agar gels (17). In general, ILC cell lines exhibited limited, dyscohesive growth in this semi-solid medium, with BCK4 cells forming the smallest colonies (Fig. 3A, top). The ILC growth was similar to the growth of MCF7 and T47D cells, the latter displaying a tighter morphology. As expected, MDA-MB-231 cells formed the most robust soft-agar colonies, serving as a positive control. Altogether, these assays indicate that ILC cells exhibit a unique anchorage-independent ability in ULA conditions, a phenotype not replicated in soft agar or mammosphere culture.

3D ECM growth and cell–matrix interactions

In tissues, ILC tumors grow as a single file of cells within a dense layer of stroma rich in ECM (1, 6). This phenomenon can be visualized by staining human tumors with Masson's trichrome,

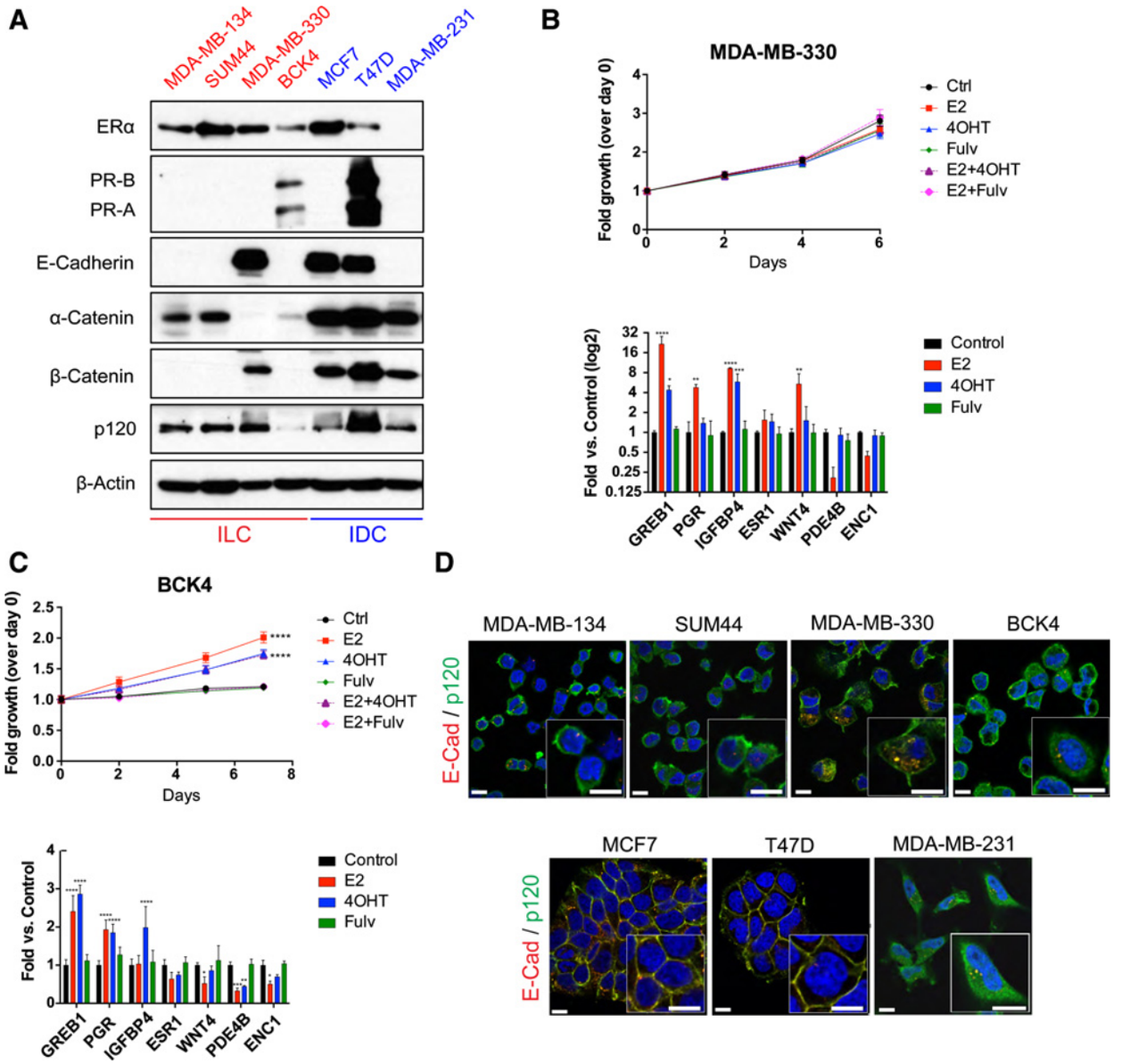

Figure 1.

Characteristics of the human ILC and IDC cell lines used in the study. **A,** Western blotting using the indicated antibodies on whole cell lysates from ILC (left; red) and IDC (right; blue) cell lines. β-Actin was used as a loading control. **B** and **C,** Time course (top) and relative ER target gene expression (bottom) after estrogen and antiestrogen treatment in hormone-deprived MDA-MB-330 (**B**) and BCK4 (**C**) cells. Graphs show representative data ($n = 6$) from two to three experiments. Control, vehicle (ethanol); E2, estradiol (100 pmol/L); 4-OHT, 4-hydroxytamoxifen (100 nmol/L); Fulv, fulvestrant (ICI 182, 780, 100 nmol/L). *P* values are from two-way ANOVA with Dunnett multiple comparison test to control. *, $P \leq 0.05$; **, $P \leq 0.01$; ***, $P \leq 0.001$; ****, $P \leq 0.0001$. **D,** Merged images and higher magnification insets of coimmunofluorescence staining for E-cadherin (red) and p120 (green) in ILC (top) and IDC (bottom) cell lines. DAPI (blue) was used for counterstaining to mark nuclei. Scale bar, 10 μm.

which clearly demonstrates higher levels of collagen fibers in ILC compared with IDC (Supplementary Fig. S4). However, the 3D ECM growth of human ILC cell lines has not previously been systematically analyzed. Therefore, we first embedded ILC cell lines in thick Collagen I gels, where MDA-MB-134 and SUM44 cells exhibited the most robust growth, while MDA-MB-330 cells displayed a looser morphology and BCK4 formed the smallest colonies (Fig. 3A). Similar results were obtained when the cells were either embedded within or cultured on top of Matrigel, displaying a "grape-like" morphology previously described for cells with poor cell–cell adhesion (42). In contrast, MCF7 and T47D cells formed very tight colonies in all ECM environments (Fig. 3B). Interestingly, MDA-MB-330 cells exhibited protrusive structures in Matrigel culture (Fig. 3A), which are more characteristic of MDA-MB-231 cells with a "stellate" morphology and known invasive potential (Fig. 3B; ref. 42).

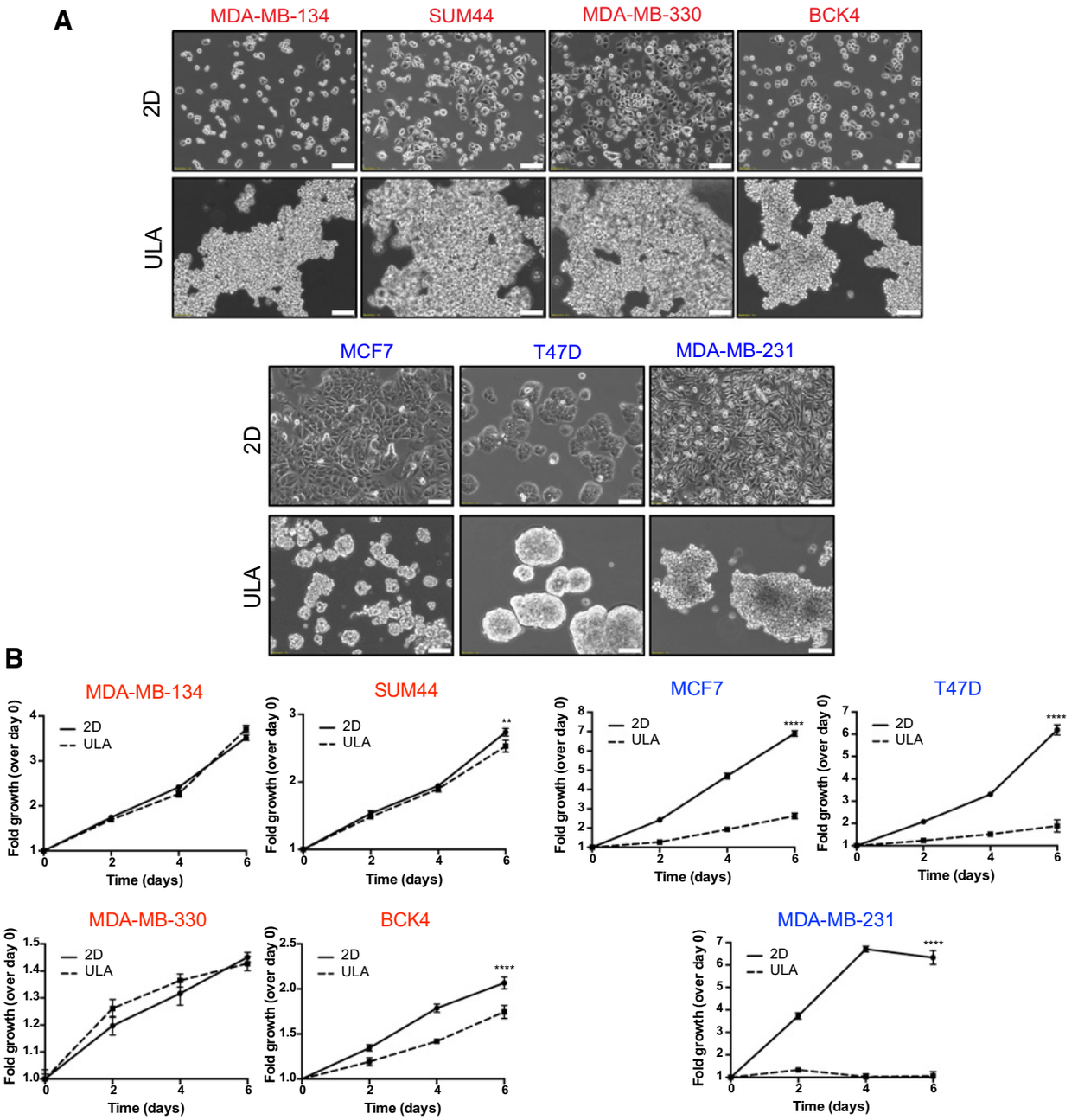

Figure 2.

Human ILC cell lines exhibit superior growth in ULA culture than human IDC cell lines. **A,** Phase contrast light microscopy images of ILC (red; top) and IDC (blue; bottom) cell lines in 6-well 2D and ULA plates 4 days postplating. Scale bar, 100 μm. **B,** Relative growth curves showing fold growth normalized to day 0 at each time point over 6 days for ILC (red; left) and IDC (blue; right). Graphs show representative data from three experiments ($n = 6$). *P* values are from two-way ANOVA comparison of 2D and ULA. *, $P \leq 0.05$; ****, $P \leq 0.0001$.

In addition to growing cells within 3D gels, we also assayed the adhesion of cells to ECM proteins in 2D to gain a deeper understanding of their cell–matrix interactions (20). To this end, we seeded ILC and IDC cell lines onto plates coated with Collagen I, Collagen IV, fibronectin, laminin, or Matrigel in serum-free media. We also utilized uncoated plates for comparison and BSA-coated plates as negative control for background adhesion levels. While a 2-hour incubation indicated a low level of overall binding in ILC cell lines, especially in MDA-MB-134 and SUM44 cells (Supplementary Fig. S5A), a 16-hour incubation resulted in more efficient binding and varying cell morphologies on different matrices (Fig. 4A; Supplementary Fig. S5B). The ECM protein most preferred for binding in general was Collagen I (Fig. 4B), on which most

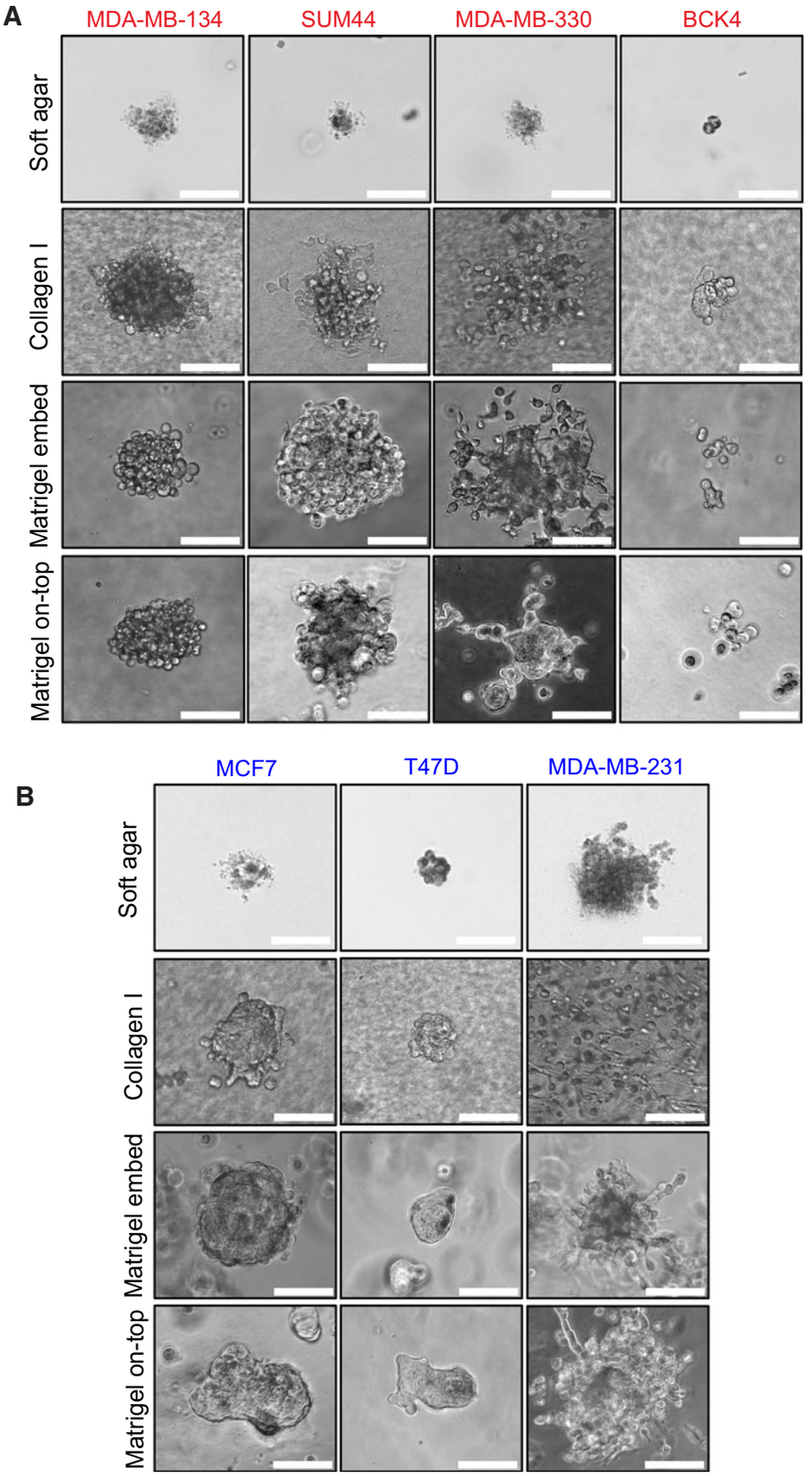

Figure 3.
ILC and IDC cell lines exhibit varying morphologies in 3D culture. Phase contrast light microscopy images of ILC (red; **A**) and IDC (blue; **B**) cell lines in soft agar (4 weeks postplating), Collagen I, Matrigel-embedded, and Matrigel on-top culture (ILC, 3 weeks postplating; IDC, 1 week postplating). Scale bar, 100 μm.

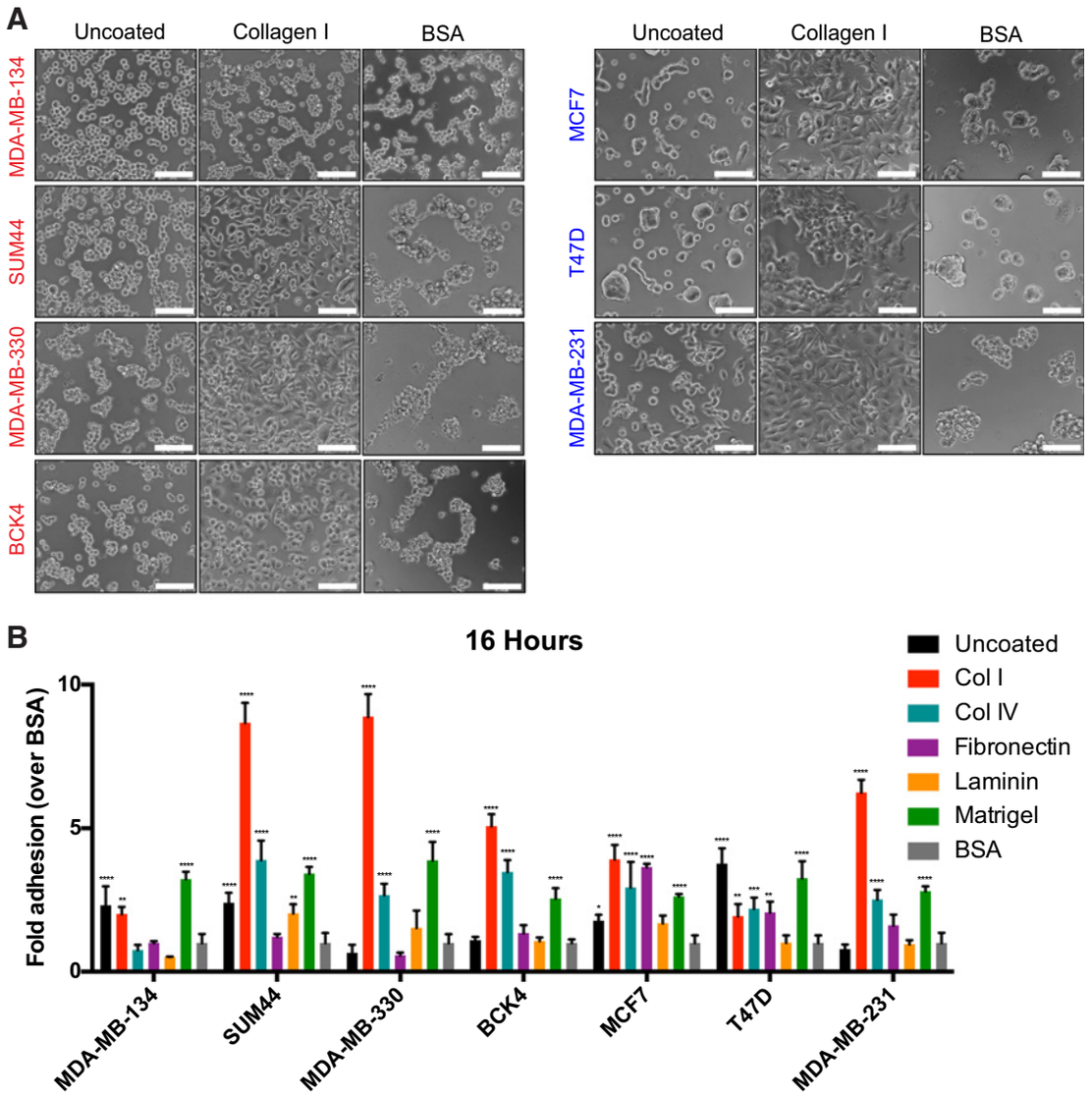

Figure 4.

Human ILC cell lines have differing preferences for adhesion to ECM proteins. **A,** Phase contrast light microscopy images of ILC (red; left) and IDC (blue; right) cell lines in uncoated, Collagen I-, or BSA-coated plates 16 hours postplating. Scale bar, 100 μm. **B,** Fold adhesion (normalized to BSA) of ILC (red) and IDC (blue) cell lines 16 hours postplating. Graphs show representative data from two experiments ($n = 4$). P values are from ordinary one-way ANOVA with Dunnett multiple comparison test to BSA for each cell line. *, $P \leq 0.05$; **, $P \leq 0.01$; ****, $P \leq 0.0001$.

cells displayed prominent spreading (Fig. 4A), followed by Collagen IV and Matrigel.

Of the ILC cell lines analyzed, MDA-MB-134 cells displayed a unique matrix interaction profile, with a less overall adhesion to ECM proteins than to uncoated plates and no visible adhesive protrusions on any matrix. Interestingly, unsupervised clustering of the ILC and IDC cell lines using publicly available transcript profiling data (32) showed that MDA-MB-134 cells clustered separately from the other ILC cell lines, displaying a unique expression pattern of genes encoding both integrins (Supplementary Fig. S5C) and matrix metalloproteinases (MMP) (Supplementary Fig. S5D), which are well known mediators of cell–matrix adhesion (20). Combined, these data indicate that ILC cell lines have differing morphologies in 3D ECM gels and divergent adhesive properties on matrix proteins.

Migration and invasion potential

Next we assessed cell migration employing the commonly used wound-scratch assay, in which a gap ("a wound") is introduced into the middle of a monolayer to induce directional movement of cells from the wound edges (21, 30). Using the IncuCyte live-cell imaging system and capturing images of cells every 4 hours, we observed very limited basal migration in the ILC cell lines (Fig. 5A, left). This was in stark contrast to the IDC cells (Fig. 5A, right), which completely closed the wound in as early as 24 hours (MDA-MB-231). To exogenously induce

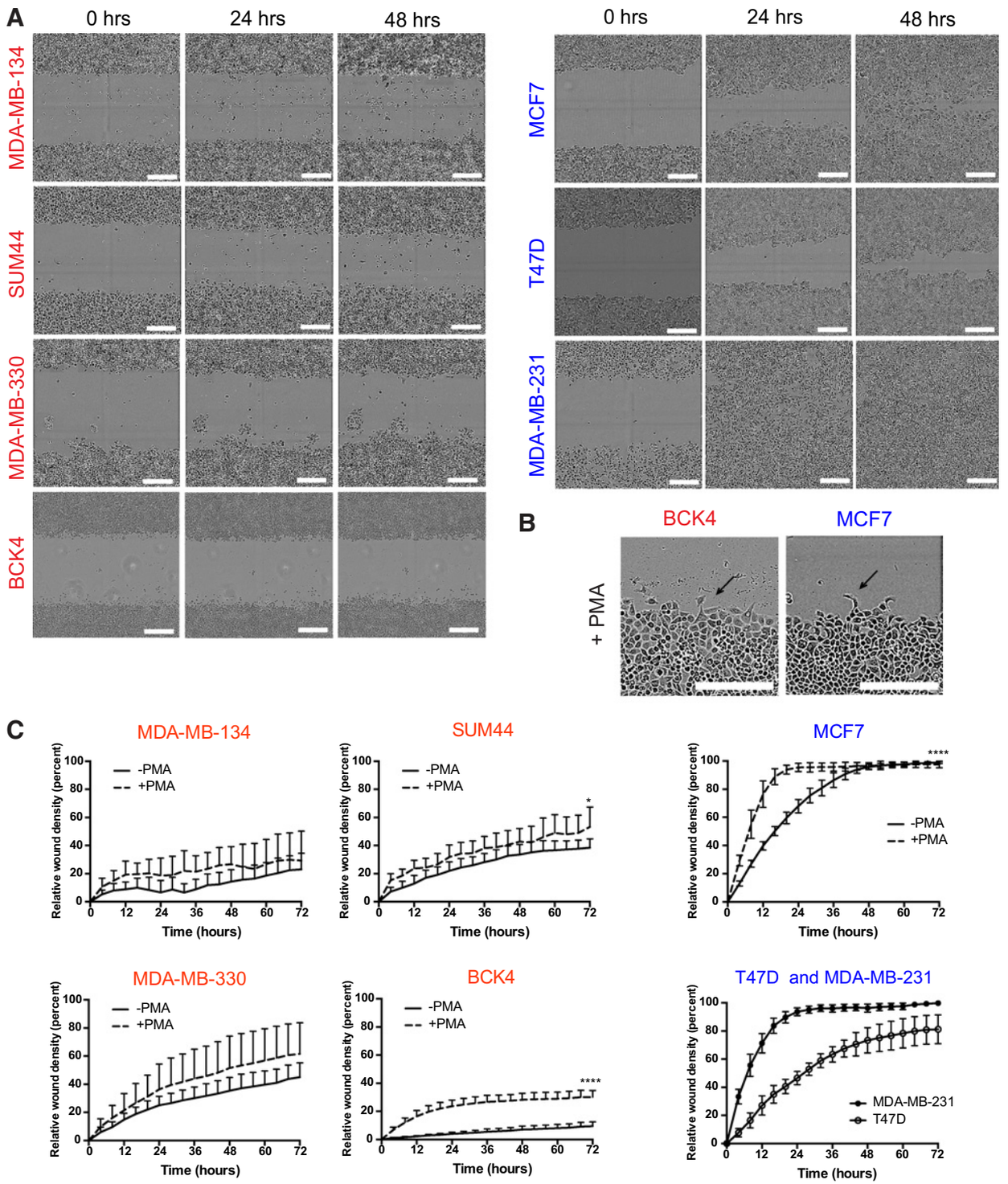

Figure 5.

Human ILC cells exhibit limited migration ability in wound-scratch assays. **A,** Snapshots of the scratch wounds in ILC (red; left) and IDC (blue; right) cell lines at the indicated time points. Scale bar, 100 μm. **B,** Snapshots of the scratch wounds in BCK4 (red) and MCF7 (blue) cell lines treated with 100 nmol/L PMA. Arrows, migratory protrusions at the wound edge. Scale bar, 300 μm. **C,** Relative wound densities over hour 0 in ILC (red; left) and IDC (blue; right) cell lines over time with and without PMA treatment. Graphs shows representative data from two to three experiments ($n = 6$–8). P values are from two-way ANOVA comparison of -PMA versus +PMA. *, $P \leq 0.05$; ****, $P \leq 0.0001$.

cell migration, we treated the cells with phorbol myristate acetate (PMA), which activates the PKC pathway and downstream actin cytoskeleton reorganization (43). PMA treatment clearly triggered migratory protrusions at the edges of the wound in MCF7 cells (Fig. 5B; right) and substantially increased their migration rate (Fig. 5C; right). In contrast, however, despite inducing protrusions in the otherwise-round ILC cell lines (Fig. 5B; left), PMA had limited effect on their movement (Fig. 5C; left). While the strongest PMA effect was in BCK4, this cell line still failed to close the wound after 72 hours.

As an alternative to the wound-scratch assay, we next utilized transwell Boyden chambers to assess migration and invasion (21). As expected, the highly migratory MDA-MB-231 cells exhibited substantial chemotaxis to FBS, while MCF7 and T47D cell were weakly migratory (Fig. 6A). However, the ILC cell lines exhibited very limited migration to FBS in this assay. Given the ECM-rich stroma of ILC tumors (see Supplementary Fig. S4; refs. 1, 6), we also assayed migration to substrate bound ECM in haptotaxis experiments (22), in which the undersides of the inserts were coated with a thin layer of Collagen I. Interestingly, SUM44 and MDA-MB-330 cells displayed abundant haptotaxis to Collagen I over BSA in this assay (Fig. 6B), despite limited chemotaxis to FBS (see Fig. 6A). This result was different from MCF7 and MDA-MB-231 cells, which exhibited Collagen I haptotaxis (Fig. 6B), but also chemotaxis to FBS (see Fig. 6A), highlighting the unique requirement of matrix only by ILC cells for migration. However, this finding did not extend to BCK4 or MDA-MB-134 cells, which did not migrate substantially in either assay (Fig. 6A and B), with the phenotype of the latter being consistent with its weak ECM adhesion (see Fig. 4).

Almost half of all human ILC tumors harbor activating, hotspot mutations in *PIK3CA* and 13% have *PTEN* loss due to inactivating mutations or deletions (7). These alterations are known to activate downstream Akt signaling, which can induce cell migration and invasion (44). While MCF7 and T47D both harbor *PIK3CA* mutations, human ILC cell lines are wild type for *PIK3CA* and *PTEN* (32). We therefore overexpressed PIK3CA mutants and knocked down PTEN in MDA-MB-134 cells to potentially augment their migration ability. Interestingly, compared with the respective controls, only the H1047R but not the E545K mutation activated downstream Akt signaling, along with all four PTEN shRNAs in MDA-MB-134 cells, which was different from the highly active MCF7 cells that harbor the endogenous E545K mutation (Supplementary Fig. S6A). However, when assayed in either transwell Boyden chambers (Supplementary Fig. S6B and S6C) or wound-scratch assays (Supplementary Fig. S6D), none of the tested alterations alone were sufficient to induce cell migration in MDA-MB-134 cells.

Using the transwell Boyden chambers, we also assayed the invasion capacity of human ILC cell lines. When plated in top chambers coated on the inside with either acid-extracted cross-linked Collagen I (Fig. 6C) or Matrigel (Fig. 6D), the highly invasive MDA-MB-231 cells were the only cell line that exhibited robust invasion; while MCF7 and T47D were weakly invasive. The ILC cell lines, however, had limited invasion of either Collagen I or Matrigel in response to FBS in bottom chambers. In addition to mesenchymal invasion of cross-linked ECM proteins, cells can also exhibit amoeboid invasion by squeezing through the pores in non-cross-linked ECM (23, 24). Given their morphologic similarity to the small, round cells of melanoma and non–small cell lung cancer that utilize amoeboid invasion, we also assayed this type of invasion in ILC cell lines using transwell chambers coated with pepsin-extracted Collagen I. In contrast to the invasive MDA-MB-231 cells; however, ILC and IDC cell lines exhibited limited amoeboid invasion in this assay (Supplementary Fig. S7A and S7B). Altogether, these results suggest that ILC cell lines exhibit limited migration and invasion in traditional laboratory assays with the exception of haptotaxis to Collagen I.

Transcriptional comparison of ILC and IDC cell lines and tumors

Our comprehensive analysis of the 2D and 3D phenotypes of human ILC cell lines clearly demonstrated unique biological properties. In order to delineate the gene expression programs that may underlie the divergent cellular phenotypes of the ILC and IDC cell lines, we performed transcriptional comparison analyses using publicly available datasets (32), which covered all of the cell lines used in this study except for BCK4. Importantly, of the ILC cell lines with available data, we only focused on MDA-MB-134 and SUM44 cells to capture the differential expression of E-cadherin in ILC versus IDC and therefore excluded MDA-MB-330 cells that do not harbor the hallmark *CDH1* mutation. In addition, ER-negative MDA-MB-231 cells were also excluded from the analyses to ensure comparison between cell lines belonging to the same molecular subtype (i.e., luminal), leaving MCF7 and T47D.

Despite the small number of cell lines analyzed, unsupervised hierarchical clustering of the ILC and IDC cells clustered MDA-MB-134 and SUM44 closer to each other and away from MCF7 and T47D (Supplementary Fig. S8A). Differential expression analysis, based on a fold-change cut-off value of 1.5 and false discovery rate (FDR) value of 0.05, identified 320 genes that were expressed higher in ILC versus IDC cell lines and 387 that were expressed lower (Fig. 7A; Supplementary Table S2). Pathway enrichment analysis on the differentially expressed genes (Supplementary Table S3) indicated upregulated transmembrane protein tyrosine kinase pathway in ILC cell lines, consisting of genes such as *FGFR1*, a known amplified oncogene in ILC (45). Additional pathways revealed from this analysis included ion channel activity, tyrosine metabolism, biological oxidation, cyclic nucleotide phosphodiesterase activity, drug metabolism cytochrome P450 and alternative cell adhesion, with genes such as *CDH2*. Conversely, the downregulated pathways confirmed the decreased intercellular junctions and proliferation in ILC versus IDC cell lines (6, 35), as well as extending to further categories such as IFN signaling, amyloids, RNA Pol I transcription, extracellular structure and organization, and focal adhesions, with the last category mediating cell–matrix interactions (Supplementary Table S3).

We recently reported a transcriptomic comparison of ILC and IDC tumors from the TCGA (7) and METABRIC (33) cohorts (27). We therefore wished to determine to what extent the *in vitro* transcriptional differences from the cell lines correlated with their *in vivo* counterpart from the tumors. To this end, we initially performed a principal component analysis of all the TCGA ER-positive, luminal A ILC ($n = 174$) and IDC ($n = 774$) tumors used in our original study (27) and the four cell lines used herein (MDA-MB-134, SUM44, MCF7, T47D), which somewhat separated the ILC and IDC tumors but clustered all the cell lines separately and away from the tumors (Fig. 7B). Nevertheless, overlap of the differentially expressed genes between ILC and IDC

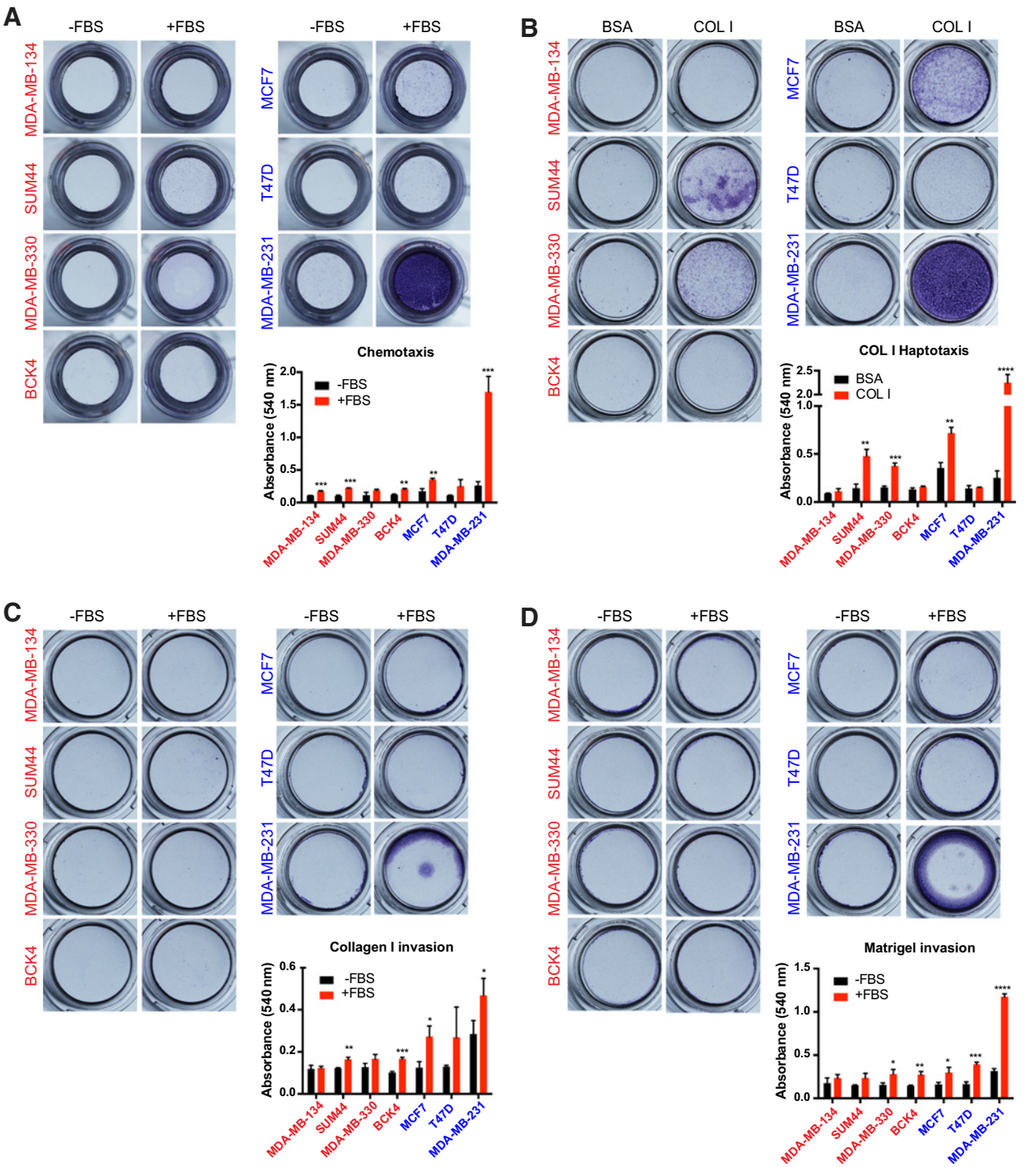

Figure 6.

Human ILC cell lines exhibit limited migration and invasion towards FBS, but SUM44 and MDA-MB-330 exhibit haptotaxis to Collagen I in transwell Boyden chamber assays. **A–D,** Images (top) and quantification (bottom) of crystal violet–stained inserts with ILC (red; left) and IDC (blue; right) cell lines from chemotaxis (**A**), haptotaxis (**B**), Collagen I invasion (**C**), and Matrigel invasion assays (**D**) toward the indicated attractants after 72 hours. Graphs show representative data from two independent experiments ($n = 3$ biological replicates). *P* values are from unpaired *t* test. *, $P \leq 0.05$; **, $P \leq 0.01$; ***, $P \leq 0.001$; ****, $P \leq 0.0001$.

tumors (27) and those between ILC and IDC cell lines (Supplementary Table S2) identified 14 commonly upregulated and 17 downregulated genes, the latter including *CDH1* (Fig. 7C; Supplementary Table S2). Importantly, a subset of these genes was also differentially regulated in MDA-MB-330 and BCK4 cells (Supplementary Fig. S8B), as well as in a recently published

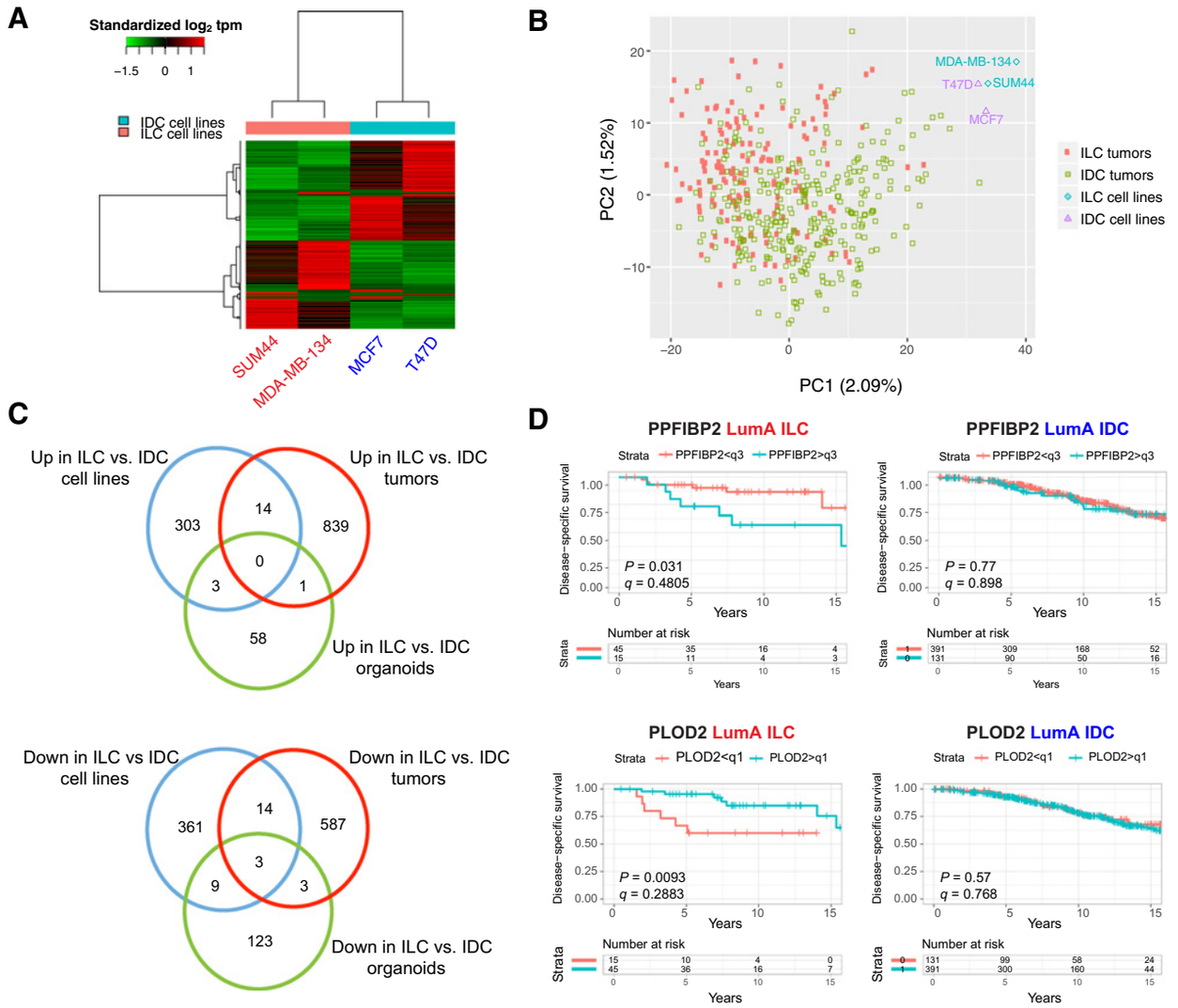

Figure 7.

Transcriptional differences between human ILC and IDC cell lines and tumors. **A,** Supervised clustering heatmap of ILC (red) and IDC (blue) cell lines using differentially expressed genes. **B,** Principal component analysis clustering plot of ILC and IDC cell lines and tumors using top 1,000 differentially expressed genes. **C,** Venn diagrams of commonly upregulated (top) and downregulated (bottom) genes between ILC and IDC cell lines, tumors, and organoids. **D,** Disease-specific survival curves for PPFIBP2 (top) and PLOD2 (bottom) in ER$^+$, luminal A ILC (red; left) and IDC (blue; right) patients in the METABRIC dataset. Patients were divided into two groups by PPFIBP2 (q3, third quadrant) and PLOD2 (q1, first quadrant) expression. *P* values are from log-rank test. *q* values were calculated using the Benjamini–Hochberg method to correct *P* values for multiple comparisons testing within histology. The small ILC sample size ($n = 60$) allows for limited statistical power in detecting survival differences after multiple testing correction.

collection of ILC organoids (Fig. 7C; Supplementary Table S2; ref. 46). The query of these genes in the METABRIC dataset (33) revealed that higher expression of *PPFIBP2*, as seen in cell lines and tumors from ILC versus IDC, was significantly associated with worse disease-specific survival in ILC but not in IDC (Fig. 7D, top). Similarly, lower expression of *PLOD2*, as seen in ILC versus IDC tumors and cell lines, exhibited a significant association with worse disease-specific survival in ILC but not in IDC (Fig. 7D, bottom). Collectively, these data highlight the subtype-specific, clinically relevant gene expression programs that may account for the divergent biological phenotypes between ILC and IDC cell lines and should be more deeply explored.

Discussion

ILC is a special subtype of breast cancer with distinct histologic and clinical features from the more common subtype IDC (1). Despite the clear need to expand our understanding of the unique biology of ILC, there are currently few laboratory models available for research and a huge gap in our knowledge on their biological properties beyond endocrine response (15). Our study is the first comprehensive report on the 2D and 3D phenotypic characterization of four ER-positive human ILC cell lines. Using a number of IDC cell lines for comparison, herein we profiled their 2D and 3D growth, matrix interactions, migratory and invasive properties

and subtype-specific gene expression programs. Although a number of ER-negative ILC cell lines are available (35), we limited our focus to the ER-positive models given that approximately 90% of ILC tumors are of this molecular subtype (1, 6). Interestingly, despite the controversial ER status of MDA-MB-330 cells (34, 35), we included them in our studies because in our hands they exhibited abundant expression of ER. Our analyses showed a lack of estrogen-induced growth in this cell line despite induction of ER target genes, while BCK4 cells exhibited a partial tamoxifen agonism similar to MDA-MB-134 cells.

The unique anchorage-independent ability we observed in the human ILC cell lines suggests resistance to anoikis (detachment-induced apoptosis), and is in agreement with findings in mouse cell lines from a transgenic model of ILC (12). Given the well-accepted role of anchorage independence in metastasis (47), our interesting result may have important clinical implications. While ILC and IDC tumors both progress to the stage of disseminated disease, patients with ILC present more often with long-term endocrine-resistant recurrences (1, 4, 5). The ability to survive in the absence of attachment to matrix may allow ILC cells to stay dormant in foreign ECM environments for extended periods of time prior to regrowth and colonization. Interestingly, our results indicated that this anchorage-independent ability was unique to the ILC cells in the ULA settings and not evident in soft-agar or mammosphere culture, suggesting a context-dependent phenotype. Importantly, based on our data, testing of therapeutic agents for ILC in future studies in both 2D and ULA conditions might allow uncoupling of potential effects on cell proliferation versus metastasis.

Our 3D ECM experiments revealed generally loose, poorly defined colonies for the ILC cell lines, which is not surprising given their defect in adherens junctions (6). Nevertheless, different cell lines still displayed varying morphologies and abilities to grow in these settings. Such a divergent pattern was especially evident in the ECM adhesion experiments, where MDA-MB-134 generally exhibited a less preference for interacting with matrix proteins. Our *in silico* analysis revealed a putative list of integrins and MMP proteins that may account for this phenotype. Interestingly, none of the ILC cell lines analyzed assumed their native, *in vivo* single-file morphology within or on top of 3D ECM gels or on 2D matrix coatings. Because the single-file pattern of the cancer cells in ILC tumors may provide important spatial and polarity cues, forcing ILC cell lines to grow in linear patterns using platforms such as micro-patterned ECM surfaces (48) may allow better modeling of ILC in the laboratory. On the basis of our data, the poor ECM adhesion of MDA-MB-134 cells makes them a less suitable choice for such future studies compared to the remaining ILC cell lines.

Given their dyscohesive morphology, we expected that ILC cell lines may exhibit single-cell migration as opposed to the collective migration of cell lines such as MCF7. To our surprise, however, in traditional wound-scratch assays, ILC cells exhibited a remarkable inability to robustly migrate even with PKC or Akt activation. This result may be due to their lack of adherens junctions, which makes it difficult to grow them into a complete monolayer and likely prevents them from experiencing the same loss of cell polarity at the wound edge as IDC cells. In transwell Boyden chambers, ILC cell lines did not exhibit substantial migration or invasion except for haptotaxis of SUM44 and MDA-MB-330 cells to Collagen I, which was consistent with their matrix adhesion properties and highlights the need for incorporating ECM proteins into such assays. While our attempts at studying amoeboid invasion of ILC cells in non-crosslinked Collagen I did not reveal much movement toward FBS, there is a clear need for more sophisticated, alternative assays using micro-patterned surfaces and stromal cell types such as fibroblasts to generate physiologically relevant confined spaces and ECM tracks (48, 49).

Our transcriptional comparison of ILC and IDC cell lines confirmed previously known differences in E-cadherin–mediated cell–cell junctions, cell proliferation, and expression of transmembrane receptor tyrosine kinases such as *FGFR1* (6, 35, 45). In addition, this analysis revealed a number of novel differences in pathways such as ion channel activity, drug metabolism cytochrome P450, and extracellular structure and organization. Interestingly, one pathway upregulated in ILC versus IDC cell lines was related to cell–cell adhesion and consisted of genes such as *CDH2*, which encodes N-cadherin. This pathway may provide alternative cell–cell communication in the absence of E-cadherin and may be indicative of a partial epithelial-to-mesenchymal transition in ILC, a result consistent with the recent RATHER report on ILC tumors (13). Collectively, the genes and pathways we identified may account for the divergent biological phenotypes of the ILC and IDC cell lines we observed throughout our studies. While this study revealed insightful data pertinent to the unique biology of ILC, we acknowledge that the cell lines used have high molecular diversity [i.e., p53 mutations despite only 4%–8% of ILCs with altered p53 (7, 13–14), K-Ras mutation in MDA-MB-134 (50) and HER2 amplification in MDA-MB-330 cells (35)], which makes it challenging to assign experimental outcomes uniquely to ILC.

Overlaying the gene expression data from ILC and IDC cell lines with that from tumors, we observed a completely separate clustering and very little overlap. This phenomenon has previously been reported for ovarian (51) and breast cancer (52), and is not surprising given the much higher complexity of *in vivo* settings compared with *in vitro* (19, 53). Future gene expression profiling studies of the cell lines cultured on ECM proteins analyzed in our study and/or in the presence of stromal cell types such as fibroblasts should yield a better recapitulation of tumor transcriptional programs. Nevertheless, our analysis identified a number of differentially regulated genes that were common between the cell lines and tumors, some of which exhibited a significant correlation with disease-free survival of patients with ILC but not IDC tumors. This approach helped generate a short list of clinically relevant genes that may be pertinent to the unique ILC biology.

PPFIBP2, also known as Liprin Beta 2, encodes a protein involved in the plasma membrane recruitment of leukocyte common antigen-related receptor (LAR) protein–tyrosine phosphatases, which regulate focal adhesions and mammary gland development (54). It is commonly fused to oncogenes such as RET in thyroid cancer and the hypomethylation of its enhancer is associated with increased breast cancer risk (55). Because our data links *PPFIB2* to poor survival specifically in the ILC cohort, further functional interrogation of this understudied, candidate oncogenic driver may implicate it as a novel therapeutic target in ILC. PLOD2 encodes an enzyme involved in the hydroxylation of lysyl residues in collagen-like peptides and ECM remodeling (56). In contrast to its promotion of metastasis in lung adenocarcinoma (57), the association of *PLOD2* with better survival specifically in the ILC cohort suggests that decreased collagen crosslinking may

create a microenvironment more permissive to growth and dissemination in ILC, underlining the importance of studying amoeboid migration and invasion.

In conclusion, our comprehensive characterization of the 2D and 3D phenotypes of ER-positive human ILC lines revealed important insights into the unique biology of ILC. With increasing interest in ILC in the laboratory and a growing list of candidate disease drivers from next-generation sequencing efforts, our study will serve as an invaluable resource for the breast cancer research community and as a platform to facilitate functional validation of potential therapeutic targets towards improving the clinical outcome of patients with ILC.

Disclosure of Potential Conflicts of Interest

No potential conflicts of interest were disclosed.

Disclaimer

The Pennsylvania Department of Health specifically disclaims responsibility for any analyses, interpretations or conclusions.

Authors' Contributions

Conception and design: N. Tasdemir, N.E. Davidson, S. Oesterreich
Development of methodology: N. Tasdemir, M.J. Sikora
Acquisition of data (provided animals, acquired and managed patients, provided facilities, etc.): N. Tasdemir, E.A. Bossart, M.J. Sikora, B.M. Jacobsen
Analysis and interpretation of data (e.g., statistical analysis, biostatistics, computational analysis): N. Tasdemir, E.A. Bossart, Z. Li, L. Zhu, M.J. Sikora, K.M. Levine, G.C. Tseng, S. Oesterreich
Writing, review, and/or revision of the manuscript: N. Tasdemir, Z. Li, M.J. Sikora, K.M. Levine, B.M. Jacobsen, G.C. Tseng, N.E. Davidson, S. Oesterreich
Administrative, technical, or material support (i.e., reporting or organizing data, constructing databases): Z. Li, S. Oesterreich
Study supervision: S. Oesterreich

Acknowledgments

The authors thank Dr. Jennifer Xavier for critical reading of the manuscript. The work is in part funded by a Department of Defense Breakthrough Fellowship Award (BC160764; to N. Tasdemir), Shear Family Foundation grant and Susan G. Komen Leadership grant (SAC160073; to S. Oesterreich), Breast Cancer Research Foundation grants (to N. Davidson and S. Oesterreich), and a grant (#4100070287) from the Pennsylvania Department of Health. E. Bossart is supported by a NIH Ruth L. Kirschstein Award (F31CA203055-01). Z. Li is supported by the University of Pittsburgh John S. Lazo Cancer Pharmacology Fellowship. M. Sikora is supported by an NIH Pathway to Independence Award (R00CA193734). K. Levine is supported by an individual fellowship from the NIH/NCI (F30 CA203154). This project used the UPMC Hillman Cancer Center Biostatistics and Tissue and Research Pathology Services (TARPS) Cores, in part supported by P30CA047904.

The costs of publication of this article were defrayed in part by the payment of page charges. This article must therefore be hereby marked *advertisement* in accordance with 18 U.S.C. Section 1734 solely to indicate this fact.

Received May 8, 2018; revised August 15, 2018; accepted September 14, 2018; published first September 18, 2018.

References

1. Rakha EA, Ellis IO. Lobular breast carcinoma and its variants. Semin Diagn Pathol 2010;27:49–61.
2. Siegel RL, Miller KD, Jemal A. Cancer statistics, 2017. CA Cancer J Clin 2017;67:7–30.
3. Evans WP, Warren Burhenne LJ, Laurie L, O'Shaughnessy KF, Castellino RA. Invasive lobular carcinoma of the breast: mammographic characteristics and computer-aided detection. Radiology 2002;225:182–9.
4. Pestalozzi BC, Zahrieh D, Mallon E, Gusterson BA, Price KN, Gelber RD, et al. Distinct clinical and prognostic features of infiltrating lobular carcinoma of the breast: combined results of 15 International Breast Cancer Study Group clinical trials. J Clin Oncol 2008;26:3006–14.
5. Metzger Filho O, Giobbie-Hurder A, Mallon E, Gusterson B, Viale G, Winer EP, et al. Relative effectiveness of letrozole compared with tamoxifen for patients with lobular carcinoma in the BIG 1–98 trial. J Clin Oncol 2015;33:2772–9.
6. McCart Reed AE, Kutasovic JR, Lakhani SR, Simpson PT. Invasive lobular carcinoma of the breast: morphology, biomarkers and 'omics. Breast Cancer Res 2015;17:12.
7. Ciriello G, Gatza ML, Beck AH, Wilkerson MD, Rhie SK, Pastore A, et al. Comprehensive molecular portraits of invasive lobular breast cancer. Cell 2015;163:506–19.
8. Rakha EA, Abd El Rehim D, Pinder SE, Lewis SA, Ellis IO. E-cadherin expression in invasive non-lobular carcinoma of the breast and its prognostic significance. Histopathology 2005;46:685–93.
9. Berx G, Cleton-Jansen AM, Strumane K, de Leeuw WJ, Nollet F, van Roy F, et al. E-cadherin is inactivated in a majority of invasive human lobular breast cancers by truncation mutations throughout its extracellular domain. Oncogene 1996;13:1919–25.
10. Berx G, Van Roy F. The E-cadherin/catenin complex: an important gatekeeper in breast cancer tumorigenesis and malignant progression. Breast Cancer Res 2001;3:289–93.
11. Derksen PW, Braumuller TM, van der Burg E, Hornsveld M, Mesman E, Wesseling J, et al. Mammary-specific inactivation of E-cadherin and p53 impairs functional gland development and leads to pleomorphic invasive lobular carcinoma in mice. Dis Mod Mech 2011; 4:347–58.
12. Derksen PW, Liu X, Saridin F, van der Gulden H, Zevenhoven J, Evers B, et al. Somatic inactivation of E-cadherin and p53 in mice leads to metastatic lobular mammary carcinoma through induction of anoikis resistance and angiogenesis. Cancer Cell 2006;10:437–49.
13. Michaut M, Chin SF, Majewski I, Severson TM, Bismeijer T, de Koning L, et al. Integration of genomic, transcriptomic and proteomic data identifies two biologically distinct subtypes of invasive lobular breast cancer. Sci Rep 2016;6:18517.
14. Desmedt C, Zoppoli G, Gundem G, Pruneri G, Larsimont D, Fornili M, et al. Genomic characterization of primary invasive lobular breast cancer. J Clin Oncol 2016;34:1872–81.
15. Sikora MJ, Cooper KL, Bahreini A, Luthra S, Wang G, Chandran UR, et al. Invasive lobular carcinoma cell lines are characterized by unique estrogen-mediated gene expression patterns and altered tamoxifen response. Cancer Res 2014;74:1463–74.
16. Rotem A, Janzer A, Izar B, Ji Z, Doench JG, Garraway LA, et al. Alternative to the soft-agar assay that permits high-throughput drug and genetic screens for cellular transformation. Proc Natl Acad Sci U S A 2015;112:5708–13.
17. Macpherson I, Montagnier L. Agar suspension culture for the selective assay of cells transformed by Polyoma virus. Virology 1964;23:291–4.
18. Lee GY, Kenny PA, Lee EH, Bissell MJ. Three-dimensional culture models of normal and malignant breast epithelial cells. Nat Methods 2007;4:359–65.
19. Stock K, Estrada MF, Vidic S, Gjerde K, Rudisch A, Santo VE, et al. Capturing tumor complexity *in vitro*: comparative analysis of 2D and 3D tumor models for drug discovery. Sci Rep 2016;6:28951.
20. Yue J, Zhang K, Chen J. Role of integrins in regulating proteases to mediate extracellular matrix remodeling. Cancer Microenviron 2012;5:275–83.
21. Justus CR, Leffler N, Ruiz-Echevarria M, Yang LV. *In vitro* cell migration and invasion assays. J Vis Exp 2014. doi: 10.3791/51046.
22. Carter SB. Haptotaxis and the mechanism of cell motility. Nature 1967;213:256–60.
23. Friedl P, Wolf K. Tumour-cell invasion and migration: diversity and escape mechanisms. Nat Rev Cancer 2003;3:362–74.
24. Sahai E, Marshall CJ. Differing modes of tumour cell invasion have distinct requirements for Rho/ROCK signalling and extracellular proteolysis. Nat Cell Biol 2003;5:711–9.

25. Jambal P, Badtke MM, Harrell JC, Borges VF, Post MD, Sollender GE, et al. Estrogen switches pure mucinous breast cancer to invasive lobular carcinoma with mucinous features. Breast Cancer Res Treat 2013;137: 431–48.
26. Fellmann C, Hoffmann T, Sridhar V, Hopfgartner B, Muhar M, Roth M, et al. An optimized microRNA backbone for effective single-copy RNAi. Cell Rep 2013;5:1704–13.
27. Du T ZL, Levine KM, Tasdemir N, Lee AV, Houten BV, Tseng GC, et al. Invasive lobular and ductal breast carcinoma differ in immune response, protein translation efficiency and metabolism. Sci Rep 2018;8:7205.
28. Manni A, Wright C, Buck H. Growth factor involvement in the multihormonal regulation of MCF-7 breast cancer cell growth in soft agar. Breast Cancer Res Treat 1991;20:43–52.
29. Lombardo Y, de Giorgio A, Coombes CR, Stebbing J, Castellano L. Mammosphere formation assay from human breast cancer tissues and cell lines. J Vis Exp 2015. doi: 10.3791/52671.
30. Liang CC, Park AY, Guan JL. In vitro scratch assay: a convenient and inexpensive method for analysis of cell migration *in vitro*. Nat Protoc 2007;2:329–33.
31. Kramer N, Walzl A, Unger C, Rosner M, Krupitza G, Hengstschlager M, et al. In vitro cell migration and invasion assays. Mutat Res 2013;752:10–24.
32. Marcotte R, Sayad A, Brown KR, Sanchez-Garcia F, Reimand J, Haider M, et al. Functional genomic landscape of human breast cancer drivers, vulnerabilities, and resistance. Cell 2016;164:293–309.
33. Curtis C, Shah SP, Chin SF, Turashvili G, Rueda OM, Dunning MJ, et al. The genomic and transcriptomic architecture of 2,000 breast tumours reveals novel subgroups. Nature 2012;486:346–52.
34. Dai X, Cheng H, Bai Z, Li J. Breast Cancer Cell Line Classification and Its Relevance with Breast Tumor Subtyping. J Cancer 2017;8:3131–41.
35. Christgen M, Derksen P. Lobular breast cancer: molecular basis, mouse and cellular models. Breast Cancer Res 2015;17:16.
36. Hollestelle A, Peeters JK, Smid M, Timmermans M, Verhoog LC, Westenend PJ, et al. Loss of E-cadherin is not a necessity for epithelial to mesenchymal transition in human breast cancer. Breast Cancer Res Treat 2013;138:47–57.
37. Shibata T, Kokubu A, Sekine S, Kanai Y, Hirohashi S. Cytoplasmic p120ctn regulates the invasive phenotypes of E-cadherin-deficient breast cancer. Am J Pathol 2004;164:2269–78.
38. Schackmann RC, van Amersfoort M, Haarhuis JH, Vlug EJ, Halim VA, Roodhart JM, et al. Cytosolic p120-catenin regulates growth of metastatic lobular carcinoma through Rock1-mediated anoikis resistance. J Clin Invest 2011;121:3176–88.
39. Zhao H, Langerod A, Ji Y, Nowels KW, Nesland JM, Tibshirani R, et al. Different gene expression patterns in invasive lobular and ductal carcinomas of the breast. Mol Biol Cell 2004;15:2523–36.
40. Bertucci F, Orsetti B, Negre V, Finetti P, Rouge C, Ahomadegbe JC, et al. Lobular and ductal carcinomas of the breast have distinct genomic and expression profiles. Oncogene 2008;27:5359–72.
41. Manuel Iglesias J, Beloqui I, Garcia-Garcia F, Leis O, Vazquez-Martin A, Eguiara A, et al. Mammosphere formation in breast carcinoma cell lines depends upon expression of E-cadherin. PLoS One 2013;8: e77281.
42. Kenny PA, Lee GY, Myers CA, Neve RM, Semeiks JR, Spellman PT, et al. The morphologies of breast cancer cell lines in three-dimensional assays correlate with their profiles of gene expression. Mol Oncol 2007;1:84–96.
43. Sumagin R, Robin AZ, Nusrat A, Parkos CA. Activation of PKCbetaII by PMA facilitates enhanced epithelial wound repair through increased cell spreading and migration. PLoS One 2013;8:e55775.
44. Samuels Y, Diaz LA Jr, Schmidt-Kittler O, Cummins JM, Delong L, Cheong I, et al. Mutant PIK3CA promotes cell growth and invasion of human cancer cells. Cancer Cell 2005;7:561–73.
45. Reis-Filho JS, Simpson PT, Turner NC, Lambros MB, Jones C, Mackay A, et al. FGFR1 emerges as a potential therapeutic target for lobular breast carcinomas. Clin Cancer Res 2006;12:6652–62.
46. Sachs N, de Ligt J, Kopper O, Gogola E, Bounova G, Weeber F, et al. A living biobank of breast cancer organoids captures disease heterogeneity. Cell 2018;172:373–86.
47. Mori S, Chang JT, Andrechek ER, Matsumura N, Baba T, Yao G, et al. Anchorage-independent cell growth signature identifies tumors with metastatic potential. Oncogene 2009;28:2796–805.
48. Paul CD, Mistriotis P, Konstantopoulos K. Cancer cell motility: lessons from migration in confined spaces. Nat Rev Cancer 2017;17:131–40.
49. Gaggioli C, Hooper S, Hidalgo-Carcedo C, Grosse R, Marshall JF, Harrington K, et al. Fibroblast-led collective invasion of carcinoma cells with differing roles for RhoGTPases in leading and following cells. Nat Cell Biol 2007;9:1392–400.
50. Turner N, Pearson A, Sharpe R, Lambros M, Geyer F, Lopez-Garcia MA, et al. FGFR1 amplification drives endocrine therapy resistance and is a therapeutic target in breast cancer. Cancer Res 2010;70:2085–94.
51. Domcke S, Sinha R, Levine DA, Sander C, Schultz N. Evaluating cell lines as tumour models by comparison of genomic profiles. Nat Commun 2013;4:2126.
52. Ross DT, Perou CM. A comparison of gene expression signatures from breast tumors and breast tissue derived cell lines. Dis Markers 2001;17:99–109.
53. Abbott A. Cell culture: biology's new dimension. Nature 2003;424:870–2.
54. Sarhan AR, Patel TR, Cowell AR, Tomlinson MG, Hellberg C, Heath JK, et al. LAR protein tyrosine phosphatase regulates focal adhesions through CDK1. J Cell Sci 2016;129:2962–71.
55. Wang Y, Hao DP, Li JJ, Wang L, Di LJ. Genome-wide methylome and chromatin interactome identify abnormal enhancer to be risk factor of breast cancer. Oncotarget 2017;8:44705–19.
56. Rautavuoma K, Takaluoma K, Passoja K, Pirskanen A, Kvist AP, Kivirikko KI, et al. Characterization of three fragments that constitute the monomers of the human lysyl hydroxylase isoenzymes 1–3. The 30-kDa N-terminal fragment is not required for lysyl hydroxylase activity. J Biol Chem 2002; 277:23084–91.
57. Du H, Chen Y, Hou X, Huang Y, Wei X, Yu X, et al. PLOD2 regulated by transcription factor FOXA1 promotes metastasis in NSCLC. Cell Death Dis 2017;8:e3143.